LASER INTERFEROMETER GRAVITATIONAL WAVE OBSERVATORY
- LIGO -
CALIFORNIA INSTITUTE OF TECHNOLOGY
MASSACHUSETTS INSTITUTE OF TECHNOLOGY

**Technical Note** **LIGO-T1600505-v1-D** 2016/11/01

# Dynamic beam profile shaping for Adaptive Optics in Advanced LIGO

M. R. Apodaca M.

*Distribution of this document:*

Detector Group

**California Institute of Technology**
**LIGO Project, MS 100-36**
**Pasadena, CA 91125**
Phone (626) 395-2129
Fax (626) 304-9834
E-mail: info@ligo.caltech.edu

**Massachusetts Institute of Technology**
**LIGO Project, NW22-295**
**Cambridge, MA 02139**
Phone (617) 253-4824
Fax (617) 253-7014
E-mail: info@ligo.mit.edu

**LIGO Hanford Observatory**
**PO Box 159**
**Richland, WA 99352**
Phone (509) 372-8106
Fax (509) 372-8137
E-mail: info@ligo.caltech.edu

**LIGO Livingston Observatory**
**19100 LIGO Lane**
**Livingston, LA 70754**
Phone (225) 686-3100
Fax (225) 686-7189
E-mail: info@ligo.caltech.edu

http://www.ligo.caltech.edu/

# 1 Abstract

In Advanced LIGO (aLIGO) absorption of the interferometer's laser in the optics causes thermal deformation that has negative effects on the interferometer's performance. Currently, aLIGO uses a thermal compensation system with a static heating beam profile to correct this deformation. Due to the constant change in thermal distortion patterns, future systems would benefit from dynamic beam shaping. An active beam shaping device is to be implemented onto the optical setup in such way that the steel mask, currently being used, will no longer be needed. A simple reflection from this device would allow us to control the intensity pattern. The main aim of this project is to implement a MEMs mirror array chip in order to have real-time control of the shape of the beam to accurately compensate the deformation of the test masses. We investigated how to program the chip and see if we could control the shape and intensity levels of the beam being reflected off this array. Testing was also done to determine the damage threshold of the chip.

# 2 Introduction

Up until now, astronomy has been based around a single wave spectrum; the electromagnetic spectrum. Nevertheless, there is one existing spectrum that not until recently we had no access to; the gravitational wave spectrum. Gravitational waves were predicted by Albert Einstein's general theory of relativity and its weak-field equation. It is believed that this radiation will provide us with different information to the electromagnetic spectrum.

Laser Interferometer Gravitational-Wave Observatory (LIGO) is, as the name implies, an experiment whose sole purpose is the detection of gravitational waves. Initial LIGO was designed to work as a Michelson's interferometer with 4 Km long arms that have Fabry-Perot cavities to increase the interaction time. It is such that at the presence of a gravitational wave one of these arms will suffer a distortion in space-time causing it to shrink while the other one stretches. This difference in arm's length then causes there to be a change in the interference pattern being detected.

However, Initial LIGO was dismantled around the year 2009 as to allow the installation of the Advanced LIGO. Although both the Initial LIGO and aLIGO there are several differences amongst them. The main difference being the better seismic isolation and the usage of a higher power laser beam. The sensitivity of the detector is determined by what is know as "the sensitivity curve". This curve plots the noise levels caused by different factors at different frequencies. These noise curves can be caused by different factors such as seismic, thermal, quantum etc. By using a higher power leads to lower quantum noise that then will increase the sensitivity of the detector at mid- and high-frequencies. Thus, aLIGO achieves better results by a factor of 10 than LIGO.

These improvements came with other problems. The higher the laser power, the greater the absorption of heat on the surface of the optics. Causing a temperature gradient on the mirror and thus causes a thermo-elastic distortion in the Fabry-Perot arms and thermo-refractivity in the recycling cavities. Therefore reducing the mode-overlap between the arm and the recycling cavities. Resulting in a loss of gravitational wave signal due to the decrease of

optical performance and sensitivity of the interferometer.

Fortunately, ALIGO thermal compensation system (TCS) is used to correct thermally-induced spatial distortions in the interferometers optical modes. The system that is currently being used consists of the use of ring heaters (RH) and a $CO_2$ laser actuator. The RH are designed to compensate for self-heating optimum power and thus reduce the temperature gradients in the mirrors. Figure 1 is a cartoon of aLIGO's TCS.

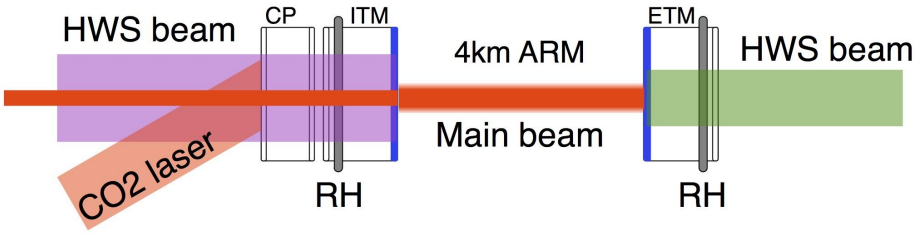


Figure 1: Cartoon showing how the Thermal Compensation System works.

However, the self-heating may be dynamic and non-uniform since there are both thermo-refractive and thermo-elastic distortion as illustrated in Figure 2. This can not be corrected for by the $CO_2$ laser actuator. The main obstacle being that the current spatial intensity shaping is done by shining the laser through a steel mask. Therefore, making it an incredibly slow process to redesign, machine and implement a new mask each time the pattern changes.

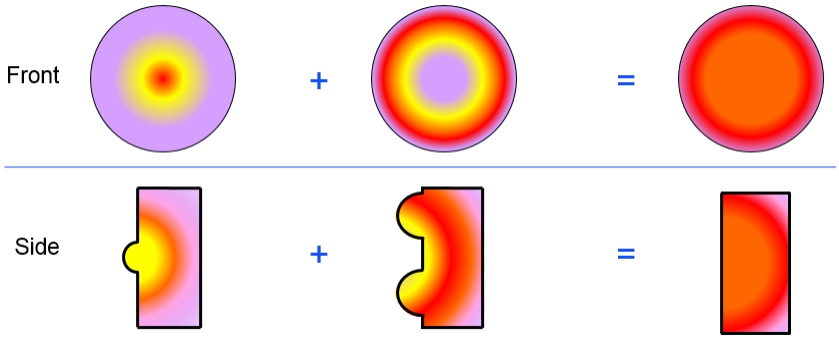


Figure 2: Cartoon showing the self heating of the optics from a frontal and side view.

The project consists on designing and developing a new generation of $CO_2$ laser projectors that can create any spatial heat distribution of the $CO_2$ laser beam in real time, to be installed in the aLIGO. Its purpose, as was the purpose of its previous generation, would be to compensate the ring heaters residual distortion. The main idea is to figure out if it is possible to use a MEMs micro-mirror array to create a real-time spatial heating profile while meeting the TCSs requirements.

# 3 Aims

- Experiments on chip:
  - Efficiency (when used with a 10.6 micron $CO_2$ Laser beam) = we need to measure the reflectivity *Background: This helps us know how much of the power is being absorbed by the MEMS array and thus calculate how much the device is to heat up*
  - damage threshold (when used with several Watts to tens of Watts of $CO_2$ laser power) *Background: see if it can resist the power of the current $CO_2$ laser currently being used. If the laser were to damage the device, then there would be no point in trying to shape the beam with a weaker laser since it would not be enough to compensate the deformation of the mirror.*
- Experiments on projector:
  - practicality of modifying the MEMs evaluation module to accept a laser beam (initially a visible, eventually a $CO_2$ laser)
  - spatial resolution: The goal is to determine the effective spatial resolution with which we can actuate on the $CO_2$ beam by using the MEMS micro-mirror array. The way the MEMS micro-mirror array is structured is by using a 608 by 648 diamond pattern geometry. This array has over 415872 mirror with a 10.8 $\mu m$ diagonal each. The way the different images are projected is by having an angle of freedom in which each individual mirror can move. In other words, each mirror can be set at a specific angle with an accuracy of 1° within a range of 24°. Background: The steel masks have limited shapes and resolution that we hope to improve with the device. Thus, it is important to know what type of patterns can be produced by using it.

# 4 Software Access and modification of the [redacted]

## 4.1 Methods

The [redacted] is a device designed by [redacted] that consists of a mirror MEMS array that is connected to a microcontroller and other optical components that combined produce images that can be manipulated straight from a computer. Throughout the program, the level of control possible of this device was studied and evaluated to see it could fit the needs of aLIGOs thermal compensation system.

Furthermore, the physical integration of the MEMS array with a $CO_2$ laser had to be engineered. This was complicated by the presence of [redacted] optical components, such as the LEDs, mirror and lens, which together helped the projector produce images in the visible.

The software interface has available several patterns and images that help the user test their device. However, it also allows the user to upload their own images and videos as long as they are in a bit map format.The layout of the software is demonstrated on Figure 4. It is also possible to upload several images that will later be available on the device, without the need of the connection to the computer. Likewise, production of our own images was tested. This was done by locating a sample code that enabled the creation of images that better fit the precision and need required by the TCS.

Figure 3: Software interface of which the [redacted] was modified from.

On the other hand, the projectors extra optical components had to be removed since they blocked the path of the $CO_2$ laser as it can be noted in Figure 3. The method consisted on removing the plastic sticker-like protection to have better visibility of the optics. It was then decided to unscrew the entire electronics off the plastic base. Once these were unscrewed, it was obvious the optics where being help in place by a black box which was screwed onto the

plate that was holding the MEMS array. This was then unscrewed. The next step was to disconnect the LEDs from the electronics. These were luckily only held down by pressure, which made it extremely easier to remove. The left over components were then reassembled and tested to confirm their functionality. Nonetheless, a new problem arose, the mirror MEMS array had a protective glass layer over it.

Figure 4: [redacted]

### 4.2 Results

The first part of the experiment was successful. The image creation of our own mathematically produced images using Matlab, combined with the possibility to upload and store several images on to the device was achieved. Making the device a good fit for the intended purposes of it as part of the TCS. Moreover, an appealing feature of the device is that these images can be accessed without the need of having to connect the [redacted] directly to the computer.

The removal of components was a complete success since the [redacted] was fully function after it was reassembled. Furthermore, it now had a clear pathway for the $CO_2$ laser to be shown onto the mirror array and the same time this was being controlled by the computer.

## 5 Glass Cover Removal

### 5.1 Methods

The existence of a protective glass layer over the mirror MEMS array represented a serious problem. The glass is a material that despite it being extremely transmitting in the visible spectra, this is not at all the case for the far infrared wavelengths. Glass is most absorbent, approximately 100%, at $10\mu m$ thus, causing the array to have 0% reflected power. Additionally, the absorbance of that much power would cause the glass mirror to burst and scratch the surface of the mirror array.

Therefore, the removal of this protective layer was of extreme importance. Before starting, the structure of the MEMS array was studied in order to determine if it were even possible to remove this cover. It was discovered that the glass was being held up by a glass frame surrounding the mirrors, to prevent them from touching, and it was being pushed down by

a sort of lever, encapsulant. This encapsulant was originally thought to be made out plastic however it was later found to be of a much stiffer and resistant material. It was believed that the best way to remove this layer was by removing the encapsulants inside a clean room in order to minimise the interaction of the mirror with outside particles that could potentially scratch the surface.

Two methods were tested in order to perfect the technique as much as possible. The first attempt was to cut through by using a scalpel. However, this method was quickly discarded considering the hardness of the material. The next idea was to file one of the encapsulants off in order to release one side of the mirror. Then, we would be able to flick off the other side of the mirror. At first, the filing was done with a normal diamond shape steal file that was later declared not strong enough and was substituted by a diamond file. With this new tool, it was possible to remove the lever and break the bond between the layer of glass and the frame. However, part of the shards of the top glass fell onto the chip and scratched the arrays mirror surface. The damage is shown on Figure 5. This led to the second attempt, filing off the lever whilst holding the chip upside down. The second attempt was successful in the sense it did not immediately scratch the surface. Nevertheless, during the transportation of the device from the clean room to the laboratory a piece of the protective glass frame broke off and scratched the surface.

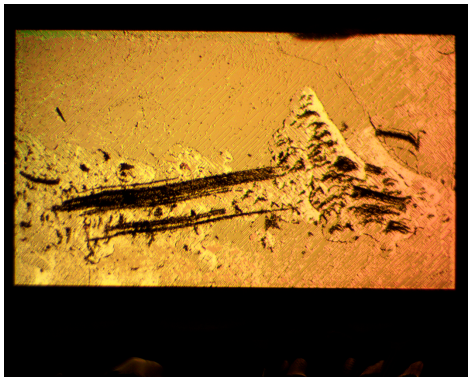

Figure 5: mirror MEMS array chip after first attempt to remove glass cover.

## 5.2 Results

The conclusion from this experiment was that although the second procedure allowed for minimal damage, the array was still being exposed to potential scratching. Thus, it was decided that the best solution would be to contact the manufacturers and ask for a special batch that instead of glass protective layers, it has zinc selenide windows. ZnSe is 100% transmitting in the far infrared making it a great substitute for the glass. On the other hand, there is also an unresolved question to face. Why two out of the three MEMS arrays when connected to the microcontroller, refuse to work after the cover was removed? It is important to note that there was not an obvious relation between the surface damage and its dysfunctionality.

# 6 Damage Testing: Temperature measurements

## 6.1 Methods

The main objective of this experiment was to detect any visible damage that may be caused by shining the $CO_2$ laser beam onto the array. It is important to monitor the increase in temperature of the chip, given that if it is to be installed in aLIGO, the chip is expected to resist up to 5W of laser power. The first part of this experiment consisted on measuring the temperature of the chip after 15s of exposure every 50mW until 400mW was reaches. This was followed by exposing the chip for 30s. The results of this are shown on Figure 6. This experiment was then repeated but instead of increasing the power, it was originally set at 400mW and the temperature was measured every minute up until 5min. The laser was then left on for 25 minutes.This enabled the measurements of the temperature after a longer period of exposure time.The results are represented on figure 7.

The optical setup for both of these experiment was the same. They consisted on a $CO_2$ laser, two mirror that helped adjust both vertically and horizontally the position of the beam being reflected on to the MEMS array that was clapped down to ensure it hit the same spot each time. The temperature readings were taken with an infrared camera.

## 6.2 Results

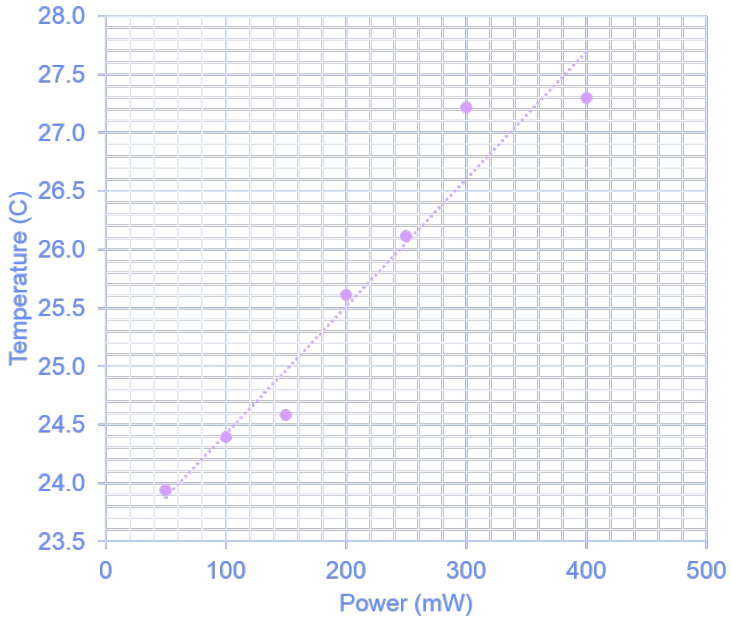


Figure 6: Graph showing temperature(C) vs. Power(mW). These are the results of the first experiment, increasing 50mW every 15s

The last experiment produced the following results:

It is important to point out that the chip which was used in this last experiment was different from the previous ones. This was the newer "less broken" chip that could give

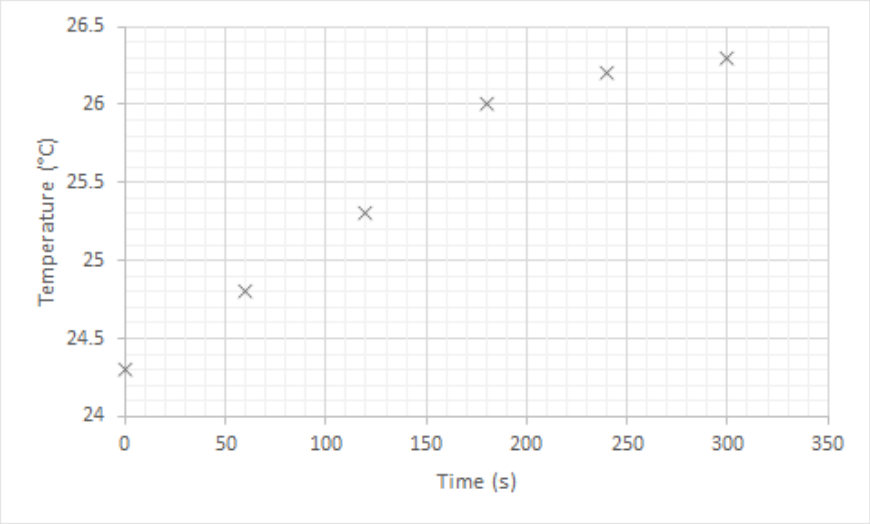


Figure 7: Graph showing temperature(C) vs. Time(s). These are the results of the second experiment, maintaining constant power (400mW)

Table 1: Damage threshold of the second MEMS array.

| | |
|---|---|
| Initial Temperature: | 23.5C |
| Final Temperature: | 25.4C |
| Input power: | 400mw |
| Output power: | 150mW |
| Total time: | 25 min |

better results. From this data the absorption coefficient was calculated to be: 0.63. This coefficient was calculated by using Table 1 and amusing that all energy that is not reflected is being absorbed. In other words:

$$\alpha = \frac{P_{in} - P_{out}}{P_{in}}$$

# 7 Intensity Patterns

## 7.1 Method - reflectivity measurement

This section of the experiment was divided into two different parts. The first part consisted of shining the visible laser onto the MEMs array while it was off in order to capture the diffraction pattern caused by the reflected beam. This measurement was done by shining the HeNe laser beam through a screen and letting this reflect off directly from the chip. This would allow to determine how much of the laser power went to the main reflected beam. This was then done with the $CO_2$ laser. The optical setup had both lasers since the HeNe laser was used to align the $CO_2$ laser. Given the damaged array was being used to do these measurements, the beam waist of both lasers had to be focused down in order to hit the undamaged sections.

## 7.2 Results - reflectivity measurements

The diffraction experiment concluded that the power being reflected of the damaged MEMs array was:

Table 2: Reflected power of the damaged MEMS array.

| Laser Type | Main Reflected Beam Power Percentage |
|---|---|
| HeNe | 60 % |
| CO2 | 58 % |

## 7.3 Method - image analysis

Considering this experiment was done with the extremely damaged array, the reflectivity measurements suggested that the MEMS array chip would be sufficiently reflected in order to be used as part of the TCS. The second part of the experiment was a lot more elaborate. The aim was to determine if it was possible to spatially modify the intensity of a laser by using the mirror array. Moreover, determine to what level of precision this could be done. The optical setup was made up of the HeNe laser and two mirrors, which allowed us to adjust with precision the position of the beam, the [redacted], iris, lens and CCD camera. The iris helped get a clearer vision by removing any noise by blocking any unwanted reflected beam from the optical components. Meanwhile, the lens help us get a sharp image since it magnified the beam in order to have a more detailed reading on the CCD camera.This optical setup is more clearly represented on Figure 8.

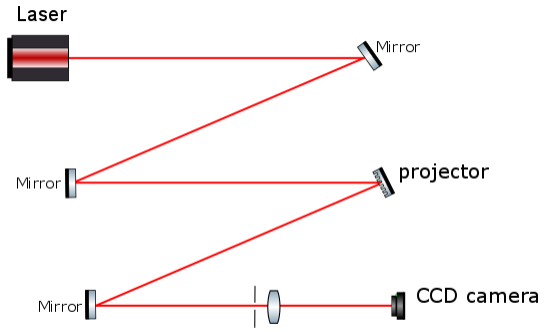


Figure 8: Visible Laser intensity measurement optical setup.

## 7.4 Results - image analysis

The images captured by the CCD camera served as evidence that the intensity could be in fact spatially modified by using the MEMS array.On Figure 9 you can appreciate from right to left how the figure is more and more detailed. However, it was not clear how precise this could be done nor if this would be equally as successful when using the $CO_2$ laser. It is important to keep in mind that the $CO_2$ laser has a much larger wavelength than that of the

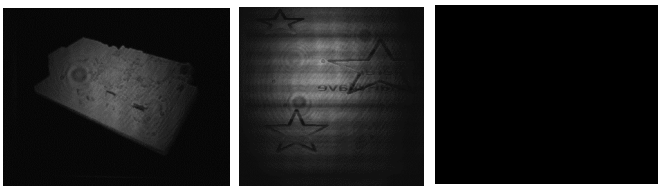

Figure 9: Different patterns produced by projecting different images on the [redacted]

HeNe. In fact, the wavelength is of the size of the mirrors on the MEMS array. Therefore, the subwavelength features of the experiment must be taken into consideration.

# 8 Intensity measurements of reflected beams

## 8.1 Methods

The optical set up used for the intensity measurements of the $CO_2$ laser and the HeNe laser were very similar.An example of his optical setup can be seen on figure 10. The optical alignment done by using the visible laser was then used to align the $CO_2$ laser. The main difference was that instead of the CCD camera, which was being used to capture the intensity changes of the HeNe laser, a Spiricon camera was placed. The original aim of the experiment was to capture the spatial deformation caused by controlling the chip. However, the goal of this experiment changed to the capture of the intensity changes caused by uploading and changing different images onto the microcontroller. This was achieved by capturing the transition of both lasers from when the chip was turned on to turned off. Once two pictures (before and during) of the transition where selected, the intensity of the lasers was compared. The first qualitative approach was to create an image using Mathlab that showed the intensity difference from both lasers. Given the different size of the detectors, the CCD camera being a lot bigger than the Spiricon, the images produced by the visible laser had to be cut. This was done in order to have a better comparison of data, since the selected area matched that captured by the Spircon.

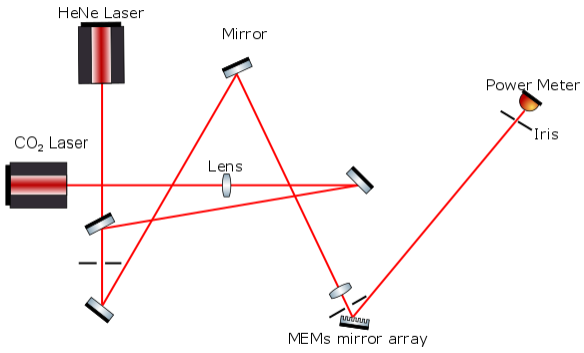


Figure 10: Intensity measurement of both visible and infrared optical setup.

Moreover, a quantitative analysis of this data was done. Each pixel of the photographs captured by the detectors was assigned a numerical value of intensity that is the associated to a colour producing the images seen in the previous experiment. Thus, allowing for a mean intensity value to be extracted from different regions of the images. By comparing how much the mean values changed for each laser before the transition and then during the transition, we can determine how effective this device is when it comes to spatially changing the intensity of the laser.

## 8.2 Results

The contrast images from both the $CO_2$ laser and the HeNe laser permitted us to identify the matching sections by comparing the patterns it produced.

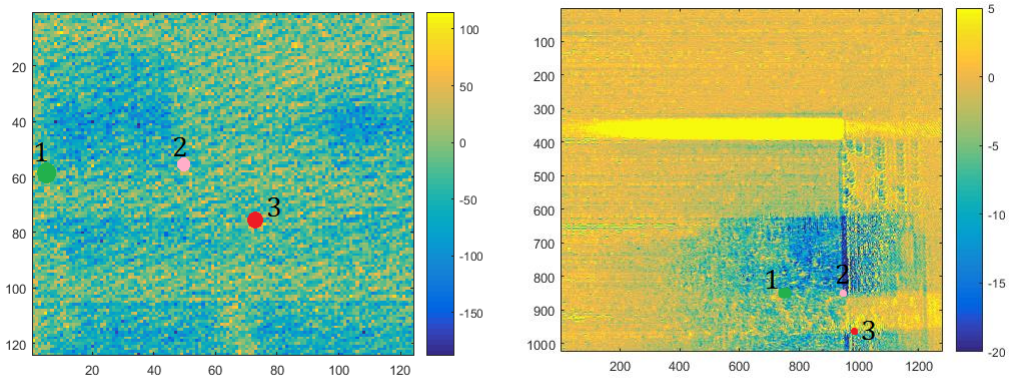


Figure 11: Original contrast Images the $10\mu m$ laser on the right and the HeNe laser on the left. The three points represent 3 matching points that helped determine the areas of interest.

Once the regions of interested where located, they were compared once again to reassure the similarities.

Furthermore, once the areas were selected, a more detailed analysis had to be done. That is, the before and during pictures of each laser were compared in order to obtain what fraction of the original intensity the second picture represented (Figure 11).

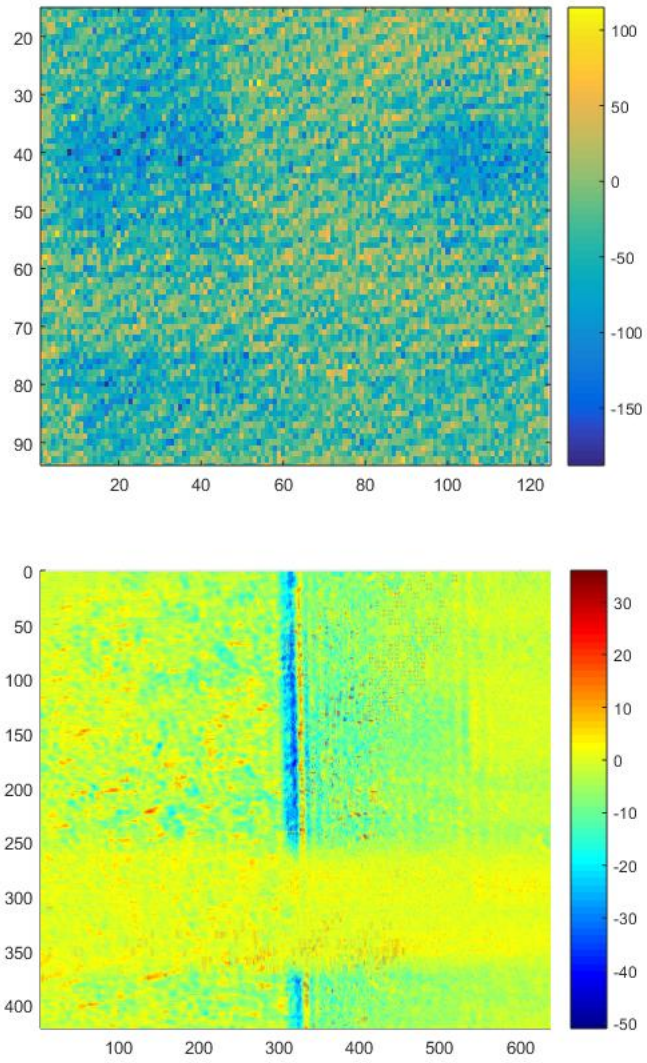


Figure 12: Related areas being compared.

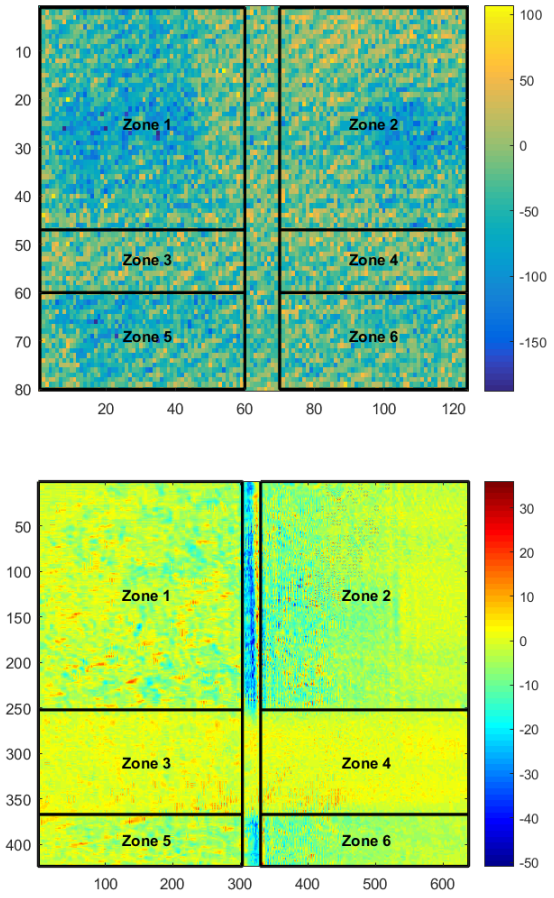


Figure 13: Selected areas of interest.

Table 3: Reflected power of the damaged MEMS array.

| HeNe: | Zone 1 | Zone 2 | Zone 3 | Zone 4 | Zone 5 | Zone 6 |
|---|---|---|---|---|---|---|
| Before: | 20.01 | 71.59 | 21.30 | 69.91 | 20.13 | 62.64 |
| After: | 16.98 | 66.85 | 21.52 | 70.08 | 17.59 | 57.65 |
| Fraction: | 0.85 | 0.93 | 1.01 | 1.00 | 0.87 | 0.92 |
| $CO_2$: | Zone 1 | Zone 2 | Zone 3 | Zone 4 | Zone 5 | Zone 6 |
| Before: | 1348 | 1431 | 1329 | 1446 | 1350 | 1455 |
| After: | 1311 | 1406 | 1289 | 1417 | 1319 | 1430 |
| Fraction: | 0.97 | 0.98 | 0.97 | 0.98 | 0.98 | 0.98 |

By seperating the data into different zones, as is shown on Figure 13 we managed to get a better idea of how great the intensity difference was depending on the location of the beam on the MEMS array. This part was very importaqnt since we expected each area to vary diferently acording to the pattern that had been programmed on to the microcontroler. From the table 3 we can se that for the HeNe laser, as some of the zones decreased in intensity, others increase. However, that was not the case of the $CO_2$ laser given that all the intensities decreased.

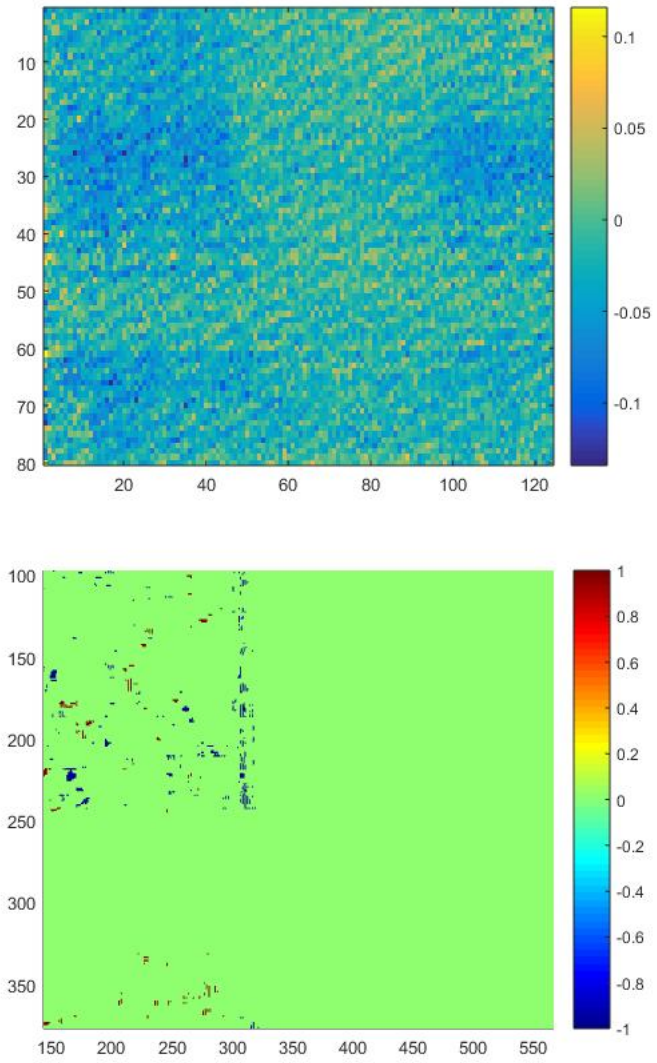


Figure 14: The intensity changes from both lasers written down as a fraction of the original intensity.

Considering the array to be at its maximum reflectivity when it is off and at its minimum during the transition. Thus, by calculating the mean out of the arrays (Figure 14), the results were that the HeNe reached a 2.34% decrease in reflectivity while the $CO_2$ laser only had a 0.13%. Meaning that the HeNe is being spatially modified approximately 18 more efficiently than the $CO_2$ laser.

# 9 Discussion

As a conclution to this proyect,

- Suggestions for protecting the chip in future installations (ZnSe = Zinc Selenide cover).
- What future damage threshold measurements are required: Allowing for the 5W on the chip for different periods of time and looking at the increase in temperature and photographing the chip under a microscope to qualitatively determine whether or not there were serious damage.
- efficiency of the reflection of the least efficient pattern
- How effective it is to upload an image real time *Try to successfully link the chip with Matlab so we can upload images a lot more efficiently. If not, make reference to the possibility of "uploading" images on the chip that can be remotely accessed with a bottom on device.*
- How conclusive do future measurements of the contrast need to be?
- How we managed to shape the image
- With proper cooling, the mems array can be used
- Future intensity noise measurements. How might these be done.

# 10 Acknowledgements

Thank you to my mentor, Aidan F. Brooks, my co-mentors Alastair Heptonstall and Gabriele Vajente, Robert Taylor, the NSF and the Caltech SURF programs.

# References

[1] LIGO, "Advanced LIGO Wiki", http://ilog.ligo-wa.caltech.edu:7285/advligo/AdvLigo

[2] A. Lazzarini and R. Weiss, "LIGO Science Requirements Document", http://www.ligo.caltech.edu/docs/E/E950018-02.pdf

[3] P. Fritschel, "DC Readout for Advanced LIGO", http://ilog.ligo-wa.caltech.edu:7285/advligo/AdvLigo

[4] http://lhocds.ligo-wa.caltech.edu:8000/mLIGO/Nonlinearity_of_the_DC_readout_signal

[5] R. Adhikari, "Sensitivity and Noise", http://www.ligo.caltech.edu/docs/P/P040032-00.pdf

[6] S. Ballmer, "LIGO Interferometer Operating as a Radiometer", http://www.ligo.caltech.edu/docs/P/P060043-00.pdf

[7] D. Sigg and J. Sidles, "Optical Torques in Suspended Fabry-Perot Cavities", http://www.ligo.caltech.edu/docs/P/P030055-C/

[8] ISC Group, "Length Sensing and Control Final Design", http://www.ligo.caltech.edu/docs/T/T980068-00.pdf

[9] ISC Group, "Interferometer Sensing and Control Conceptual Design", http://www.ligo.caltech.edu/docs/T/T070068-00.pdf

[10] P. Fritschel, "LIGO", http://arxiv.org/abs/0711.3041

[11] M. Evans, "Optickle", http://www.ligo.caltech.edu/docs/T/T070260-00.pdf

[12] M. Evans, "Optickle (LSC talk)", http://www.ligo.caltech.edu/docs/G/G070728-00

[13] [redacted]

[14] Brooks, A.f., *The Advanced LIGO Thermal Compensation System*

[15] Ramette, J, Kasprazack, M, Brooks A.F. et al (2015), *Analytical Model for Ring Heater Thermal Compensation in Advanced LIGO*

[16] Aasi, J, Abbott, B.P. et al (2015), *Advanced LIGO, Classical and Quantum Gravity,* ,Volume 32, Number 7

[17] [redacted]

[18] [redacted] User's Guide, [redacted]

[19] [redacted] *Kit*, [redacted]

[20] *The Properties of Optical Glasses* https://books.google.com/books?id=J0RX1mbhz AEC&pg=PA90&lpg=PA90&dq=transmission+spectra+of+glass&source=bl&ots=0GQuJyslN8&sig=f

[21] Brooks, Aidan, Heptonstall, Alistair (2012) *TCS beam shaping: optimum and achievable beam profiles for correcting thermo-refractive lensing (not thermo-elastic surface deformation)*

[22] Kogelnik, H., Li, T. *Laser Beams and Resonators*

# A Interferometer Parameters

| | |
|---|---|
| ITM Transmission | 0.01 |
| ITM imbalance ($T_{ITMX} - T_{ITMY}$) | $T_{ITM}/50$ |
| Average round trip arm loss | 75 ppm |
| Differential arm loss | 30 ppm |
| Beamsplitter R/T imbalance | $\pm 5 \times 10^{-3}$ |
| Differential arm offset from dark fringe | 12 pm |
| Output mode cleaner finesse | 500 |

Table 4: Parameters used in the Optickle modeling. Shown are those parameters that determine the laser and modulation source noise couplings.

# B Interferometer Strain Noise Spectrum

Each ISC technical noise source (such as laser frequency noise) must be controlled to be no greater than 1/10-th of the interferometer target strain noise spectrum, at all frequencies. The target strain noise is calculated with Bench, v6.2, and is shown in Fig. **??**. The Bench output for this curve is:

| | |
|---|---|
| Laser Power: | 125.00 Watt |
| SRM Detuning: | 8.30 degree |
| SRM transmission: | 0.12 |
| ITM transmission: | 0.010 |
| PRM transmission: | 0.0318 |
| Finesse: | 623.64 |
| Power Recycling Factor: | 33.03 |
| Arm power: | 819.57 kW |
| Power on beam splitter: | 4128.59 W |
| BNS Inspiral Range: | 173.61 Mpc |
| BBH Inspiral Range: | 1032.03 Mpc |
| Stochastic Omega: | 2.13e-009 |